Hybrid virtual polarimetric massive MIMO measurements at 1.35 GHz

Frédéric Challita, Pierre Laly, M. Lienard, Emmeric Tanghe, Wout Joseph, Davy Gaillot

Hybrid Virtual Polarimetric Massive MIMO Measurements at 1.35 GHz

Frédéric Challita[1*], *Pierre Laly*[1], *Martine Liénard*[1], *Emmeric Tanghe*[2], *Wout Joseph*[2], *Davy P. Gaillot*[1]

[1] *University of Lille, IEMN, Bâtiment P3,Villeneuve d'Ascq, 59655*
[2] *IMEC-WAVES, Ghent University, Ghent, Belgium*
** E-mail: frederic.challita@univ-lille.fr*

Abstract: The polarimetric massive MIMO radio channel of an indoor Line-Of-Sight (LOS) scenario is investigated at 1.35 GHz using a real-time radio channel sounder. The 8×12 massive MIMO transmitter is constructed using a hybrid architecture including a vertical uniform linear array (V-ULA) translated at different horizontal positions forming a virtual, yet realistic, uniform rectangular array. The performance of the system is evaluated with 6 users distributed in the room for different polarization schemes and receiver orientations using propagation channel-based metrics (such as receiver spatial correlation, Rician factor, etc.) and system-oriented metrics such as sum-rate capacity and signal to interference and noise ratio. The results show a clear dependence of the performance to the polarization schemes and receiver orientation. Furthermore, it is concluded that the additional degree of freedom brought by the polarization diversity can contribute to improve spectral efficiency, paving the way for further capacity enhancements in massive MIMO systems.

1 Introduction

New radio requirements and challenges are arising in the near future for modern telecommunication systems [1]. These requirements include increased capacity, improved data rate, decreased latency, and better quality of service [2] for scenarios and use-cases outlined in [3]. To meet these demands, drastic improvements need to be made in the cellular network architecture. Massive MIMO is a multi-user MIMO (MU-MIMO) system using spatial multiplexing over a wireless channel and is considered as one of the emerging 5G technologies capable of filling the gap between current telecommunication standards and these future requirements for next generation wireless systems. This concept was first introduced in [4] where the author states that as the base station (BS) antennas approach infinity, individual user channels become spatially decorrelated and pair wise orthogonal. An overview of benefits, opportunities and challenges for massive MIMO are presented in [5–7]. Different pre-coding techniques are studied in [8] and it was concluded that, in the studied residential-area environment, users can be uncorrelated using reasonably large number of antennas combined with simple linear pre-coders. A comparison between the performance of the different pre-coders is presented for massive MU-MIMO systems in [9].

However, characterizing a full physical massive MIMO radio channel can be a complex and costly approach. Large-scale MIMO channel sounding and system evaluation have only been tested in some labs [10–14] and a few field trials were reported such as in [15–17]. The largest gains in a massive MIMO setup come from spatial multiplexing of many users per cell, thus these gains can only be harvested when there are many users simultaneously requesting data. Recently, the Russian telecom operator MTS has deployed more than 40 state-of-the-art LTE sites with massive MIMO functionality in seven cities where the 2018 FIFA World Cup took place [18].
Another popular sounding solution is virtual measurements of massive MIMO wherein one antenna moves over several positions to simulate a full system. However, in a virtual setting approach, mutual coupling between different antennas is overlooked as well as RF chains imperfections and power consumption issues. In addition, since the measurement time can well exceed the coherence time due to the displacement of the antenna, only static radio channels can be investigated. In [19], a LOS scenario was studied for an indoor environment at 94 GHz with a focus on spatial correlation and phase variations. In [20], a virtual ULA of 128 positions (spanning 7.4 m) was used for outdoor measurements at 2.6 GHz with vertically polarized antennas. In [21], a virtual circular array has been investigated in an actual indoor environment at 20 GHz and channel measurements with statistical modeling of virtual 2D massive MIMO UWB (ultra wideband) channels are reported for two typical indoor environments using virtual elements were reported in [22]. In [23], propagation characteristics of a virtual massive MIMO (256×16) in an urban macro cell scenario were investigated at 3.5 GHz with 100 & 200 MHz bandwidths and 6 GHz with 200 MHz bandwidth. Other indoor measurements were also conducted at 6 GHz [24], 13-17 GHz [25] and some mobile measurements for cluster variation were reported in [26]. Other outdoor measurements exist also in the literature at 15 GHz [27] and 3.33 GHz [28]. All these measurements evaluate the massive channel using metrics such as eigenvalue distribution, condition number, Rician factor, delay spread and other system metrics such as sum-rate capacity.

Nonetheless, there is a clear lack in the literature regarding polarimetric massive MIMO measurements and the potential of using polarization diversity as an additional degree of freedom to improve orthogonality between the different channels. This possibility depends on the channel characteristics underlining the importance of exploiting channel parameters such as the Rician factor and the cross-polarization discrimination factor.

This work falls within this context and aims at experimentally evaluating the polarimetric 96×6 massive MIMO channel in an indoor scenario at 1.35 GHz where all 6 users are equipped with a single antenna. As such, this configuration can alternatively be categorized under the MU-MISO type (multiple-input single-output) which is expected to be deployed in practice. The massive MIMO transmitter is a hybrid virtual setup and consists in a real V-ULA translated at different horizontal positions. This is a trade-off between a full virtual setup and a full physical array. This approach is rather original for massive MIMO systems as far as the authors are concerned and its benefits are discussed later. The massive multi-user channel is extracted for different user orientations using the real-time channel sounder MIMOSA (Multiple-Input Multiple-Output Sounding Acquisition) [29]. System performance for different polarization schemes (co- and cross-polarization) is evaluated using propagation and system metrics. Zero-forcing (ZF) is used for pre-coding and the iterative waterfilling technique for power allocation. This combination is emerging as a popular approach for

massive MIMO systems [30–34]. In particular, the capability of a massive MIMO system to spatially separate a given number of users and the sum-rate capacity in the studied indoor environment are addressed for the different setups.
The rest of the paper is organized as follows: the system model and pre-coding techniques are outlined in section II. Section III presents system performance metrics and propagation channel evaluation tools. In section IV, the scenario, measurement setup and the channel sounder are presented. Before concluding, the different results are presented in Section V.

1.1 Notations

In this paper, $\mathcal{E}\{.\}$ denotes the mathematical expectation, $(.)^H$ represents the Hermitian matrix (conjugate transpose), $|.|$ is the absolute value (magnitude), $\|.\|$ the norm of a vector and $\|.\|_F$ denotes the Frobenius norm of a matrix. $\det$ is the determinant of a matrix and Tr its trace. Lower case letters are used to denote scalars, upper case boldface letters represent matrices and boldface is used to denote vectors. $\sim \mathcal{CN}(\mu, \sigma^2)$ denotes a complex circular symmetric Gaussian distribution with mean μ and variance σ^2. I.i.d. denotes the independent and identically elements distribution.

2 System model

2.1 System Model

Here, for post-processing the results, only the downlink (DL) channel of a massive MU-MISO system is considered. The BS is equipped with M antennas serving simultaneously and in the same time-frequency resource K single-antenna users distributed in the scenario. The channel can be described as flat-band at each subcarrier or frequency point. The received signal at user k is given by:

$$y_k = \mathbf{h}_k \mathbf{w}_k {s'}_k + \sum_{i=1,\, i\neq k}^{K} \mathbf{h}_k \mathbf{w}_i {s'}_i + n_k, \tag{1}$$

where y_k is the received DL signal for user k, $\mathbf{H}$ is the composite $K \times M$ channel matrix and $\mathbf{h}_k \in \mathcal{C}^{1\times M}$ is the k^{th} complex raw vector of $\mathbf{H}$ from the M BS antennas towards user k and $\mathbf{n}$ the white-noise vector with i.i.d. circularly-symmetric complex Gaussian $\mathcal{CN}(0, \sigma_n^2)$ elements. In Eq. 1, $\mathbf{W}$ denotes the $M \times K$ pre-coding matrix formed by the beamforming vectors for each user $\mathbf{W} = [\mathbf{w}_1, \mathbf{w}_2, ..., \mathbf{w}_K]$.

$$\mathbf{s}' = \sqrt{\mathbf{P}}\mathbf{s}, \tag{2}$$

where $\mathbf{s}$ is the $K \times 1$ data symbol raw vector with unit energy ($\mathcal{E}(\mathbf{s}\mathbf{s}^H) = 1$). In this case, $\mathcal{E}(\mathbf{s}'{\mathbf{s}'}^H) = P_T$ where $\mathbf{P}$ is the diagonal $K \times K$ power allocation matrix with diagonal elements p_k designating power allocated to the k^{th} user subject to the total available power P_T constraint:

$$\sum_{k=1}^{K} p_k \leq P_T. \tag{3}$$

It should be noted that if both $\mathbf{W}$ and $\mathbf{n}$ have unit power (given that $\mathbf{s}'$ has also unit energy), p_k can be interpreted as transmit signal to noise ratio (SNR) after the normalization. In this investigation, the well-known water-filling iterative algorithm is used for power distribution. The water-filling approach has been widely used to optimize power allocation amongst users in massive MU-MISO schemes [35–37].

2.2 Pre-coding techniques

Pre-coding techniques are designed for separating spatial data streams while minimizing inter-user interference as much as possible. Massive MIMO benefits derive from the use of linear pre-coders [4] such as MRT, ZF, and MMSE (or regularized ZF). For DL, the base station pre-filters signals to the intended users. The performance of the different pre-coders depends on the considered scenario, the generated channels, the number and distribution of users and other factors.
In this investigation, only ZF will be evaluated and is given by Eq. 4:

$$\mathbf{W} = \mathbf{H}^H(\mathbf{H}\mathbf{H}^H)^{-1} \;\; for\; ZF \tag{4}$$

The normalized version of each pre-coding vector is given by $\frac{\mathbf{w}_k}{\|\mathbf{w_k}\|}$.

3 System Performance and Propagation Channel Evaluation

3.1 System Performance

In order to evaluate the system performance, the sum-rate capacity with water-filling is used. Indeed, sum-rate capacity provides an upper bound on the achievable rates and spectral efficiency aspect. Moreover, it is considered that the computation of the optimal sum capacity is a particularly complex task since the power allocation needs to be numerically optimized. This clearly shows the benefit of linear schemes alongside heuristic strategies such as water-filling in practice. This is specifically true for large-scale MIMO systems for which channel hardening [38] is more pronounced compared to classical MIMO systems. Taking into account Eq. 1, the corresponding signal to interference plus noise ratio ($SINR$) for user k is given by:

$$SINR_k = \frac{p_k |\mathbf{h}_k \mathbf{w}_k|^2}{\sum_{i=1,\, i\neq k}^{K} p_i |\mathbf{h}_k \mathbf{w}_i|^2 + \sigma_n^2}, \tag{5}$$

It should be noted that ρ is included in the water-filling optimization so its value is underlying in p_k. The corresponding rate for user k is:

$$C_k = \log_2(1 + SINR_k), \quad in\; bits/s/Hz \tag{6}$$

and the sum-rate in the considered cell or scenario will be:

$$C = \sum_{k=1}^{K} C_k. \tag{7}$$

3.2 Propagation Channel Characteristics

In order to characterize the behavior of the different polarization schemes XY (where X is the polarization at Tx (H or V) and Y is the polarization at the Rx (H or V)), the average received power $\mathcal{P}(\psi)$ is first computed in the bandwidth B_w for each Tx-Rx link at each snapshot N and for every polarization link ψ. ψ could be either co-polar ($X = Y$) or cross-polar ($X \neq Y$). The power per link and snapshot is expressed as:

$$\mathcal{P}(\psi) = \frac{1}{M_f} \sum_{i=1}^{M_f} (|\mathbf{h}(\psi, \mathbf{i})|^2), \tag{8}$$

where $\mathbf{h}(\psi, \mathbf{i})$ represents the complex transfer function at frequency point i for a given polarization link ψ and M_f the number of frequency points. In this polarimetric investigation, it is critical to characterize the channel depolarization effects to understand the different mechanisms impacting the system performance. Cross-polarization discrimination (XPD) is defined as the ratio between average received power in co-polarization mode to the average received power in cross-polarization mode and can be expressed as :

$$XPD(dB) = 10\log_{10}\left(\frac{\mathcal{P}^{co-polar}}{\mathcal{P}^{cross-polar}}\right). \tag{9}$$

Also, the Rician factor K, defined as the ratio between the LOS and MPC (multipath components without the LOS component)

power (Eq. 10), a classical parameter in wireless communication systems, is here studied. Its influence on spatial correlation (defined below) and system performance is evaluated for LOS environments where users separation (and pre-coding weights) is more complex than in rich-scattered Rayleigh environment.

$$K(\text{dB}) = 10\log_{10}\left(\frac{P_{LOS}}{\sum_{i=1}^{N} P_{NLOS}^{i}}\right), \quad (10)$$

where P_{LOS} is the LOS power, P_{NLOS}^{i} is the power of the i^{th} NLOS MPC, and N the number of computed NLOS MPC.

3.3 Spatial Channel Correlation

The Rx spatial correlation properties highlight the capability of a massive MU-MISO system to simultaneously serve a number of users. It evaluates the orthogonality between channel vectors and thus reflects if the propagation is favorable or not. The propagation is said to be favorable when users are mutually orthogonal (thus an environment with rich scattering). In Massive MIMO, it is more adequate to talk about joint correlation of multiple channel vectors (a channel vector is a $1 \times M$ vector containing the channels for the M element array to a given user). First, the receiving correlation matrix $\mathbf{R_{Rx}}$ can be expressed as:

$$\mathbf{R_{Rx}} = \mathcal{E}\{\mathbf{H}\mathbf{H}^{H}\}, \quad (11)$$

and then normalized with the corresponding variances of the channel vectors. In order to represent the result of the operation in Eq. 11, a scalar value for ρ_{Rx} should be derived. A macroscopic Rx correlation coefficient ρ_{Rx} (or intercorrelation) is derived from $\mathbf{R_{Rx}}$ by averaging the off-diagonal upper triangular part of $\mathbf{R_{Rx}}$ (because of Hermitian symmetry). The canonical model in the Massive MIMO literature is i.i.d. Rayleigh fading. In this case the vector is a circularly symmetric complex Gaussian random variable. With i.i.d. Rayleigh fading, the channel gain $\|\mathbf{h}\|^2$ follows an Erlang distribution (scaled χ^2 distribution) where the channel direction $\mathbf{h}/\|\mathbf{h}\|$ is uniformly distributed over the unit sphere in $\mathbb{C}^M$. This is a spatially uncorrelated channel model that will be used throughout the investigation as a reference model.

4 Measurement Setup and Channel Sounder

4.1 Measurement setup and scenario

The static indoor office scenario is located on the University of Lille campus in the building hosting the IEMN-TELICE research group. The office dimension is 7.92 m x 6.82 m x 3 m (W x L x h). The room is surrounded by concrete walls on all sides and furnished with wooden tables disposed as shown in the panoramic view (Fig. 1) from the transmitter array point of view. 6 Rx users with single (bi-polar) antenna each are considered. The entrance is through a wooden door and the schematic in Fig. 2 gives a detailed view of the Rx distribution in the room. The location of the Rx users was chosen randomly but some are close users (i.e. spatially correlated which are presumably harder to separate). The metallic radiator protection covers the whole wall along D under four windows. The channel sounder was in the room while the measurements were performed. As it can be seen, a LOS always exists between Tx and Rx to simulate a strong Rician environment.

4.2 Radio Channel Sounder and Hybrid Setup

The MIMOSA radio channel sounder used to measure the radio channel transfer functions has been developed jointly by the TELICE group of the University of Lille and the WAVES group of the University of Ghent. This sounder allows the simultaneous measurement of 16 outputs and 16 inputs over an 80 MHz bandwidth at 1.35 GHz central frequency. The sounder allows real-time processing of transfer matrices which are measured in $\sim 200\ \mu s$. Technical and detailed specifications of the sounder can be found in [29].

Fig. 1: Panoramic view of the indoor room from the HV-MMIMO transmitter.

The massive transmitter array consists in an 8-element vertical ULA (V-ULA) fixed on an 80 cm long metallic rail equipped with a motor commanded via a LabView positioning program. By specifying (1) the horizontal step and (2) the number of desired positions for the V-ULA, a hybrid massive array setup can be configured. This is a simple and practical solution to test a massive MU-MISO system that does not require the full number of radio frequency chains. It is also a faster approach than a full virtual system with one displaced element along x and y direction and for which coupling effects and RF impairments are totally neglected. The link between the LabView program and the motor is done using optical cables such that the computer can be located outside of the room. The full simulated 96 elements array is shown as in Fig. 2. The first V-ULA position is shown on the right and the 11 other positions are represented with faded colors.

Identical dual-polarized patch antennas are used for Tx and Rx. These antennas operate at 1.35 GHz with 80 MHz bandwidth, 80 degrees beamwidth at -3 dB (in azimuth and elevation), 7 dBi gain and typical nominal VSWR ≤ 2 in the band of interest [39]. In these polarimetric measurements, each Tx-Rx link will have four channels formed by the combination of 4 different polarization schemes : VV and HH for co-polarization, VH and HV for cross polarization. Note that in optimal conditions, the Tx inter-element spacing for the ULA should be equal to the horizontal displacement. However, the specified step for the positioning program is in hexadecimal format and a precise value could not be reached resulting in a negligible a 3.7 $\%$ error between vertical and horizontal spacing. Main features of the channel sounder as well as the hybrid setup parameters of the Tx array are listed in Table 1.

Four different orientations O were selected for the measurements as depicted in Fig. 2 : ($O1$) facing the board (A side), ($O2$) facing the entrance door (B), ($O3$) facing the back wall (C) and ($O4$) facing the windows (D). For the following analysis, all antennas representing user equipments have the same orientation.

5 Results

5.1 Propagation Channel Characteristics

The empirical cumulative distribution function (ecdf) of the average received power (see Eq. 8) for each orientation O and for all four possible polarization links ψ is presented in Fig. 3 to illustrate the power variation between the different scenarios. First, it can be seen that $O1$ and $O2$ display the highest average received power because they are facing (for all users except Rx3 in $O1$) the transmitting array. $O3$ and $O4$ display ≈ 3 dB less received power. It can also be concluded that V and H polarization both propagate equally well in this scenario with no significant difference. Hence, only the V-polarization for reception will be considered in order to simplify the analysis but both polarizations at Tx are considered. This assumption derives from a practical point of view where the complexity of switching polarizations is at the Tx side.

Table 1 Radio channel sounder main features and System Parameters

MIMOSA Main Features		Tx array parameters	
Frequency	1.35 GHz	# of ULA elements	8
Span BW	80 MHz	# of horizontal positions	12
Resolution (sampling step)	12.5 ns (3.75 m)	# of Tx antennas M (hybrid setup)	96
Dynamic Range	$>$ 100 dB	# of Rx users K	6
Frequency points	819	Antenna spacing for ULA	10.8 cm (0.486 λ)
Subcarrier spacing	97.7 kHz	Horizontal Step	10.368 cm (0.468 λ)
Wavelength	22.22 cm		
Snapshot time	243.84 μs	Height of first Tx element	1.01 m
Number of snapshots	10	Height of last Tx element	1.765 m
Tx output power	0.01 to 1 W	Height of Rx antenna	1.65 m
Number of snapshots	10	Number of orientations	4

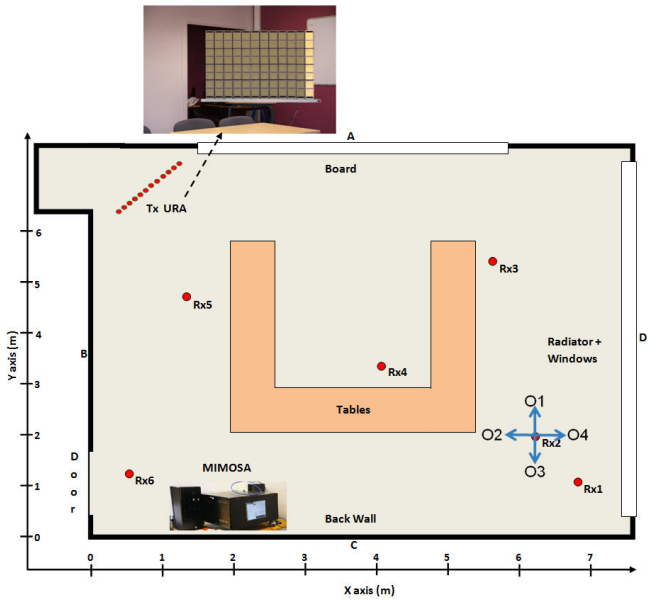

Fig. 2: Schematic top-view of the indoor room and the Tx setup

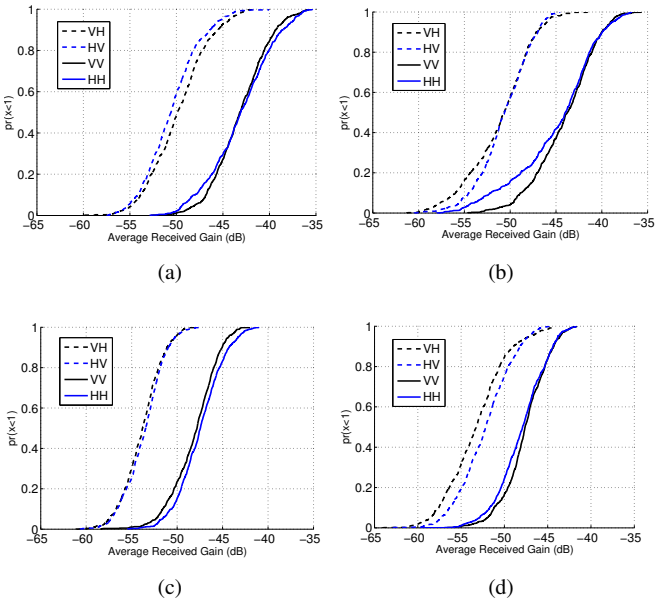

Fig. 3: Average received gain for all four orientations and all polarization links: a) O1, b) O2, c) O3, d) O4.

Table 2 Median received power for different selected configurations

Orientation	ψ	$\mathcal{P}(\psi)$(dB)
$O1$	VV	-43.11
	HV	-50.6
$O2$	VV	-43.77
	HV	-50.61
$O3$	VV	-47.81
	HV	-53.46
$O4$	VV	-47.62
	HV	-52.17

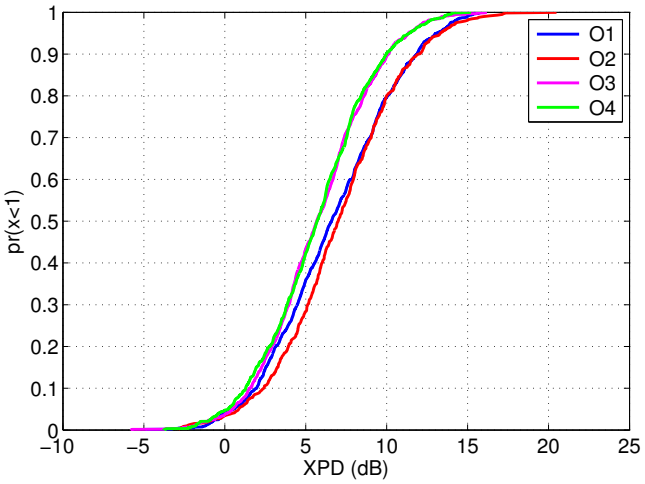

Fig. 4: ECDF of the XPD for all four orientations.

In addition, Fig. 4 presents the XPD (VV/HV) for all four orientations. The corresponding values of median values for average received power for the considered scenarios are shown in Table 2. The XPD values vary between -3 and 20 dB for $O1$ and -6 and 16 dB for $O3$. Two close families of curves appear for $O1/O2$ and the other for $O3/O4$, respectively. These differences justify the analysis as a function of different orientations to inject diversity in the observed channels for the same indoor scenario.

5.2 Rice Factor

The ecdf of K, averaged over different snapshots and users, is shown in Fig. 5. From this figure, it can be seen that K varies between $\approx$ 3.5 and 12.3 dB for 50% of the values underlining a considerable difference between the users channels for different orientations and links. Also, $O1$ and $O2$ experience a stronger Rician environment than $O3$ and $O4$ suggesting more correlation between users and specifically for co-polarization schemes could be reached. For $O1$ and $O2$, the gap between co and cross-polarized curves ($\approx$ 3 - 4 dB) is greater than for $O3$ and $O4$ for which VV and HV schemes

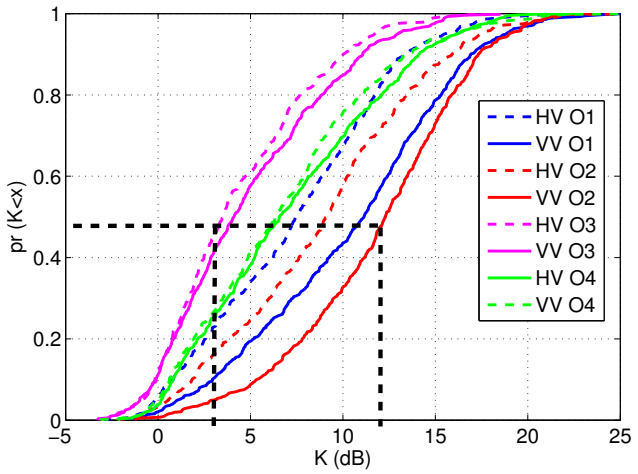

Fig. 5: ECDF of Rician factor K for all four orientations.

display similar values. For $O3$ and $O4$ presenting smaller values of K (weaker LOS), polarization diversity does not affect the Rician factor. Hence, the dependence of polarization diversity to spatial separation between users might be expected to less pronounced than $O1$ and $O2$.

5.3 Spatial Receiver Correlation

ρ_{Rx} (Eq. 11) is presented in Fig. 6 as a function of the number of active Tx antennas for all orientations and for VV and HV polarization. The results indicate that ρ_{Rx} strongly depends on the user orientation O. In addition, for a given O, ρ_{Rx} strongly depends on ψ. For $O3$ and $O4$, values of ρ_{Rx} are slightly lower for co-polarization schemes and more importantly drop faster. This means that less Tx antennas are needed to decorrelate the users in the scenario with proper pre-coding. Moreover, for $O3$, the correlation curve for the cross-polarized scheme exhibits higher values than $O4$. This might be due to the fact that the Rx antenna for $O3$ is facing the back wall in some positions (Rx 1,2 and 6) causing strong reflections contributing to the channel correlation and decreasing the Rician factor K as observed in Fig. 5.

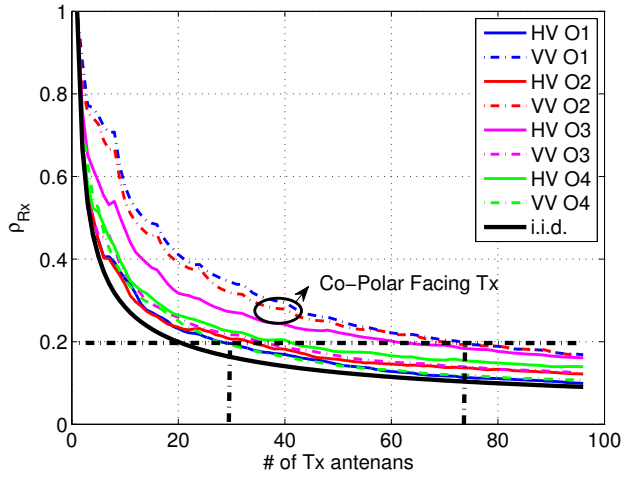

Fig. 6: Receiver spatial correlation for all four orientations and HV/VV polarizations.

The highest observed values of ρ_{Rx} correspond to the co-polar schemes in $O1$ and $O2$ which display a LOS with higher average received power compared to $O3$ and $O4$ (Fig. 3) and higher Rician factors (Fig. 5). From this point of view, better propagation conditions for massive MIMO are obtained for $O3$ and $O4$. However, for $O1$ and $O2$, the lowest values of ρ_{Rx} are observed for the cross-polarization links. Hence, it follows a better spatial separation is obtained to enhance the system performance even under strong LOS conditions using only polarization diversity. It is noteworthy that the number of Tx antennas might be large for such indoor scenarios at the chosen frequency range. However, due to the simplicity and practicality of the hybrid setup, the selected number of Tx antennas is not an issue and consequently may allow verifying the asymptotic behavior of massive MU-MISO channels with respect to the canonical model.

Reducing the number of radio frequency chains (provided that antenna selection strategies are deployed at system level), is a critical topic. Here, and for a desired correlation value threshold, the correlation results indicate that the number of active antennas can be optimized for a given orientation and polarization scheme. For example, it can be observed for $\rho_{Rx} = 0.3$ that no more than 40 antennas are needed for the worst case (upper curve) and 12 antennas for the best case. However, to reach smaller values such as 0.2, polarization diversity is clearly observed as an additional degree of freedom to reduce the number of needed active antennas (30 for HV vs. 75 for VV in $O1$). It is also observed from Fig. 6 that the difference between two polarization schemes for a given orientation O depends on the Rician factor K and the XPD factor illustrated in Fig. 5 and 4, respectively. For instance, the larger the difference in K values between co and cross-polarization schemes (see $O1$ and $O2$ in Fig. 5), the larger the gap between the corresponding configurations for ρ_{Rx}. This suggests a clear relationship between the contribution of the MPC (strong K variations) and the evolution of ρ_{Rx} for different schemes ψ.

5.4 Sum Rate Capacity

In this section, the aim is to evaluate the sum-rate capacity of the system and address the key points of this investigation : 1) the influence of polarization diversity on the performance of the system, 2) the ZF performance for different polarization schemes and 3) the trade-off between low correlation values and high channel gains. Indeed, a full polarimetric modeling of the massive MU-MISO channel is still missing and the purpose of this study is to demonstrate the necessity to develop such models including polarization diversity.

The results of sum-rate capacity defined in Eq. 7 for ZF with waterfilling power allocation are discussed in this section with $\sigma_n^2 = 1$. First, it has to be mentioned that the presented results include averaging over either SNR or number of Tx antennas and also depend on several parameters such as the power allocated, actual channel gain, spatial receiver correlation, orientation and polarization schemes. In Fig. 7, the sum-rate capacity is plotted as a function of the number of the number of Tx antennas and averaged over the SNR range ([-5 30 dB]) after the normalization process.

Similarly to the correlation results, the data clearly indicate that a better performance is obtained with $O3$ and $O4$ compared to $O1$ and $O2$. Indeed, as shown previously, $O3$ and $O4$ exhibit favorable propagation conditions despite a lower received power on average. Also, $O4$ performs better than $O3$ and $O1$ better than $O2$ which presents the strongest LOS component because it is facing the array for all users. It is important to underline an analogy between Fig. 7 and Fig. 6. For $O3$ and $O4$, VV polarization works better than HV. For $O1$ and $O2$, HV polarization presents higher values of capacity. This shows a relationship between spatial correlation and sum-rate capacity for ZF. In strong Rician environments (high channel gains) such as in $O1$ and $O2$, using cross-polarization will not only cause a drop in the users channel vectors correlation, but will also yield to an increase in the sum-rate capacity and overall spectral efficiency improvement.

This fact establishes a trade-off between low correlation values and high channel gains. In Fig. 8, the sum-rate capacity is plotted as a function of the SNR averaged over the range of Tx antennas.

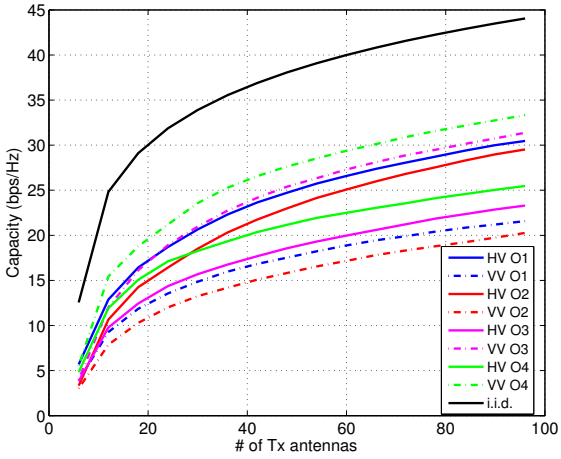

Fig. 7: Sum-rate capacity = f(M) for ZF with waterfilling.

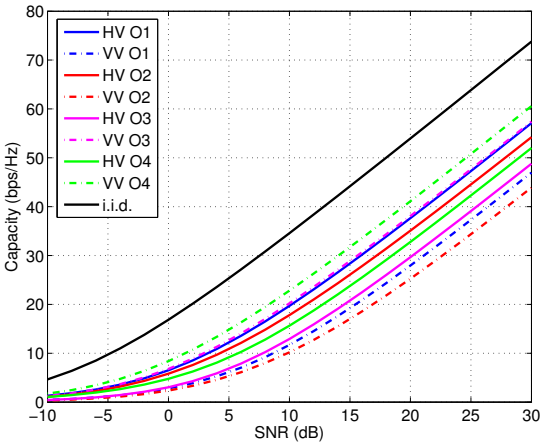

(a)

Fig. 8: Sum-rate capacity = f(SNR) for ZF.

It can be seen that sum-rate capacity varies linearly with SNR, especially for large SNR values and reaches very good values compared to the i.i.d. curve. The order of the curves is similar to that in Fig. 7 and the same conclusions stand. For instance, in Fig. 8, the curves are close to each other and schemes with lower correlation values result into better sum-rate capacity. However, the gap trends in Fig. 5 and 6 are not observed for sum-rate capacity results. This is due to the application of the waterfilling technique for which power is not evenly distributed among users and, therefore, affects the overall sum-rate capacity. Under this umbrella, equal power allocation was considered to evaluate the effect of polarization diversity for different orientations (Fig. 9). Evidently, the obtained values are lower because this allocation strategy is not optimal (especially for low SNRs). However, the gaps between curves are in agreement with those observed for the Rician factor and spatial correlation values. For $O3$ and $O4$, wherein a lower average K is experienced and a narrower difference between co and cross-polarized schemes is reached, polarization diversity effects are not well pronounced. For $O1$ and $O2$, the wider gap in K between co and cross-polarization is shown to result in lower spatial correlation values as discussed earlier. Thus, the overall sum-rate capacity for these configurations is improved.

Finally, it is noteworthy that the overall performance is not solely dependent on K as the average received power and XPD also contribute. However, it can be safely concluded from the presented results the importance of full polarimetric modeling of the massive MU-MISO channel if benefits are to be harvested from polarization diversity.

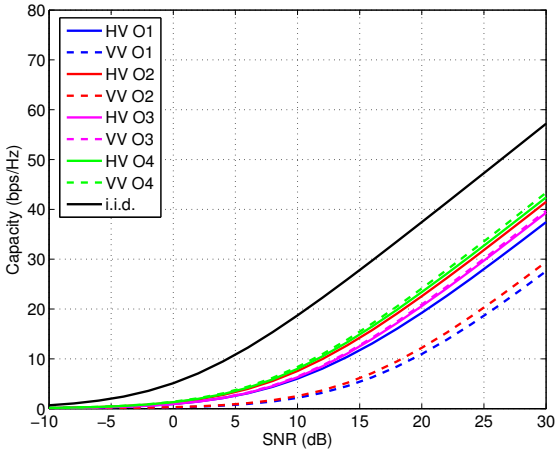

(a)

Fig. 9: Sum-rate capacity = f(SNR) for ZF and equal power allocation.

6 Conclusion

In this contribution, polarimetric massive MU-MISO measurements were performed with a real-time channel sounder at 1.35 GHz over a 80 MHz bandwidth with a large 8×12 URA for Tx and 6 Rx users under four different orientations in an indoor scenario. The massive channel was evaluated using propagation characteristics such as average received power, XPD and Rician factor K. Moreover, the spatial correlation was evaluated for all orientations and polarization schemes. It was observed that the correlation varies as a function of the orientation and the polarization schemes. Cross-polarized schemes have better spatial separation than co-polarized schemes for orientations where a strong LOS component is present. On the other side, system performance was evaluated via sum-rate capacity using ZF linear pre-coder and compared with the spatially uncorrelated i.i.d. canonical model. From this analysis, cross-polarized schemes were shown to perform better with ZF and waterfilling when spatial correlation is correspondingly lower. The additional degrees of freedom brought by polarization diversity alongside spatial multiplexing were demonstrated to enhance the system capacity and improve spectral efficiency. Future works include polarimetric massive MU-MISO measurements in outdoor and industrial scenarios to validate the conclusions of this work.

ACKNOWLEDGEMENT

This work was funded through the OS4 SMARTIES research program by the ELSAT2020 project co-financed by the European Union with the European Regional Development Fund, the French state and the Hauts de France Region Council.

7 References

1 P. Pirinen, "A brief overview of 5g research activities," in *1st International Conference on 5G for Ubiquitous Connectivity*, Nov 2014, pp. 17–22.

2 A. Gupta and R. K. Jha, "A survey of 5g network: Architecture and emerging technologies," *IEEE Access*, vol. 3, pp. 1206–1232, 2015.

3 A. Osseiran, F. Boccardi, V. Braun, K. Kusume, P. Marsch, M. Maternia, O. Queseth, M. Schellmann, H. Schotten, H. Taoka, H. Tullberg, M. A. Uusitalo, B. Timus, and M. Fallgren, "Scenarios for 5g mobile and wireless communications: the vision of the metis project," *IEEE Communications Magazine*, vol. 52, no. 5, pp. 26–35, May 2014.

4 T. L. Marzetta, "Noncooperative cellular wireless with unlimited numbers of base station antennas," *IEEE Transactions on Wireless Communications*, vol. 9, no. 11, pp. 3590–3600, November 2010.

5 F. Rusek, D. Persson, B. K. Lau, E. G. Larsson, T. L. Marzetta, O. Edfors, and F. Tufvesson, "Scaling up mimo: Opportunities and challenges with very large arrays," *IEEE Signal Processing Magazine*, vol. 30, no. 1, pp. 40–60, Jan 2013.

6 L. Lu, G. Y. Li, A. L. Swindlehurst, A. Ashikhmin, and R. Zhang, "An overview of massive mimo: Benefits and challenges," *IEEE Journal of Selected Topics in*

Signal Processing, vol. 8, no. 5, pp. 742–758, Oct 2014.
7 E. G. Larsson, O. Edfors, F. Tufvesson, and T. L. Marzetta, "Massive mimo for next generation wireless systems," *IEEE Communications Magazine*, vol. 52, no. 2, pp. 186–195, February 2014.
8 X. Gao, O. Edfors, F. Rusek, and F. Tufvesson, "Linear pre-coding performance in measured very-large mimo channels," in *Vehicular Technology Conference (VTC Fall), 2011 IEEE*, Sept 2011, pp. 1–5.
9 M. Ju, J. Qian, Y. Li, G. Tan, and X. Li, "Comparison of multiuser mimo systems with mf, zf and mmse receivers," in *2013 IEEE Third International Conference on Information Science and Technology (ICIST)*, March 2013, pp. 1260–1263.
10 S. Malkowsky, J. Vieira, L. Liu, P. Harris, K. Nieman, N. Kundargi, I. C. Wong, F. Tufvesson, V. Owall, and O. Edfors, "The world's first real-time testbed for massive mimo: Design, implementation, and validation," *IEEE Access*, vol. 5, pp. 9073–9088, 2017.
11 P. Harris, W. B. Hasan, S. Malkowsky, J. Vieira, S. Zhang, M. Beach, L. Liu, E. Mellios, A. Nix, S. Armour, A. Doufexi, K. Nieman, and N. Kundargi, "Serving 22 users in real-time with a 128-antenna massive mimo testbed," in *2016 IEEE International Workshop on Signal Processing Systems (SiPS)*, Oct 2016, pp. 266–272.
12 J. Vieira, S. Malkowsky, K. Nieman, Z. Miers, N. Kundargi, L. Liu, I. Wong, V. ï£¡wall, O. Edfors, and F. Tufvesson, "A flexible 100-antenna testbed for massive mimo," in *2014 IEEE Globecom Workshops (GC Wkshps)*, Dec 2014, pp. 287–293.
13 Titan, *TitanMIMO*, 2015, https://www.nutaq.com/5g-massive-mimo-testbed.
14 C. Shepard, H. Yu, N. Anand, E. Li, T. Marzetta, R. Yang, and L. Zhong, "Argos: Practical many-antenna base stations," in *Proceedings of the 18th Annual International Conference on Mobile Computing and Networking*, ser. Mobicom '12. New York, NY, USA: ACM, 2012, pp. 53–64. [Online]. Available: http://doi.acm.org/10.1145/2348543.2348553
15 Samsung, *Samsung and Sprint Conduct Real-World Massive MIMO Testing at Mobile World Congress Fall 2017*, 2017, https://insights.samsung.com/2017/09/11/samsung-and-sprint-conduct-real-world-massive-mimo-testing-at-mobile-world-congress-fall-2017/.
16 DeutscheAG, "Berlin trial shows throughput boost," https://www.telekom.com/en/media/media-information/consumer-products/berlin-trial-shows-throughput-boost-503698, 2018, accessed: 2018-05-08.
17 Telkomsel and ZTE, "Telkomsel and zte complete fdd-lte massive mimo field trial," https://www.telegeography.com/products/commsupdate/articles/2017/07/14/telkomsel-and-zte-complete-fdd-lte-massive-mimo-field-trial/, 2018, accessed: 2018-04-30.
18 Ericsson, "Ericsson and mts to deliver superior mobile broadband experiences for football fans at tournament in russia," https://www.ericsson.com/en/press-releases/2018/6/ericsson-and-mts-to-deliver-superior-mobile-broadband\-experiences-for-football-fans-at-tournament-in-russia, 2018, accessed: 2018-07-08.
19 F. Challita, M. Martinez-Ingles, M. Liénard, J. Molina-Garcia-Pardo, and D. P. Gaillot, "Line-of-sight massive mimo channel characteristics in an indoor scenario at 94 ghz," *IEEE Access*, pp. 1–1, 2018.
20 X. Gao, O. Edfors, F. Rusek, and F. Tufvesson, "Massive mimo performance evaluation based on measured propagation data," *IEEE Transactions on Wireless Communications*, vol. 14, no. 7, pp. 3899–3911, July 2015.
21 R. Kataoka, K. Nishimori, N. Tran, and T. Imai, "Basic performance of massive mimo in indoor scenario at 20-ghz band," in *2015 International Symposium on Antennas and Propagation (ISAP)*, Nov 2015, pp. 1–4.
22 Y. Zahedi, R. Ngah, R. Abdolee, and D. W. Matolak, "Characterization of massive mimo uwb channel for indoor environments," in *2017 IEEE 13th Malaysia International Conference on Communications (MICC)*, Nov 2017, pp. 57–62.
23 Z. Zheng, J. Zhang, Y. Yu, L. Tian, and Y. Wu, "Propagation characteristics of massive mimo measurements in a uma scenario at 3.5 6 ghz with 100 200 mhz bandwidth," in *2017 IEEE 28th Annual International Symposium on Personal, Indoor, and Mobile Radio Communications (PIMRC)*, Oct 2017, pp. 1–5.
24 J. Li, B. Ai, R. He, Q. Wang, B. Zhang, M. Yang, K. Guan, and Z. Zhong, "Directional analysis of indoor massive mimo channels at 6 ghz using sage," in *2017 IEEE 85th Vehicular Technology Conference (VTC Spring)*, June 2017, pp. 1–5.
25 J. Chen, X. Yin, and S. Wang, "Measurement-based massive mimo channel modeling in 13 -17 ghz for indoor hall scenarios," in *2016 IEEE International Conference on Communications (ICC)*, May 2016, pp. 1–5.
26 C. Wang, J. Zhang, L. Tian, M. Liu, and Y. Wu, "The spatial evolution of clusters in massive mimo mobile measurement at 3.5 ghz," in *2017 IEEE 85th Vehicular Technology Conference (VTC Spring)*, June 2017, pp. 1–6.
27 J. Chen, X. Yin, X. Cai, and S. Wang, "Measurement-based massive mimo channel modeling for outdoor los and nlos environments," *IEEE Access*, vol. 5, pp. 2126–2140, 2017.
28 D. Fei, R. He, B. Ai, B. Zhang, K. Guan, and Z. Zhong, "Massive mimo channel measurements and analysis at 3.33 ghz," in *2015 10th International Conference on Communications and Networking in China (ChinaCom)*, Aug 2015, pp. 194–198.
29 P. Laly, "Sondeur de canal mimo temps rÃl'el et applications," Ph.D. dissertation, 2016, thèse de doctorat dirigÃl'e par LiÃl'nard, Martine Micro et nanotechnologies, acoustique et tÃl'lÃl'communications Lille 1 2016. [Online]. Available: http://www.theses.fr/2016LIL10168
30 S. Jin, X. Wang, Z. Li, and K. Wong, "Zero-forcing beamforming in massive mimo systems with time-shifted pilots," in *2014 IEEE International Conference on Communications (ICC)*, June 2014, pp. 4801–4806.
31 L. D. Nguyen, T. Q. Duong, H. Q. Ngo, and K. Tourki, "Energy efficiency in cell-free massive mimo with zero-forcing precoding design," *IEEE Communications Letters*, vol. 21, no. 8, pp. 1871–1874, Aug 2017.
32 A. K. Papazafeiropoulos, H. Q. Ngo, and T. Ratnarajah, "Performance of massive MIMO uplink with zero-forcing receivers under delayed channels," *CoRR*, vol. abs/1607.06351, 2016. [Online]. Available: http://arxiv.org/abs/1607.06351
33 D. Qiao, W. Tan, Y. Zhao, C. Wen, and S. Jin, "Spectral efficiency for massive mimo zero-forcing receiver with low-resolution adc," in *2016 8th International Conference on Wireless Communications Signal Processing (WCSP)*, Oct 2016, pp. 1–6.
34 C. Zhang, Y. Jing, Y. Huang, and L. Yang, "Performance analysis for massive MIMO downlink with low complexity approximate zero-forcing precoding," *CoRR*, vol. abs/1711.00415, 2017. [Online]. Available: http://arxiv.org/abs/1711.00415
35 N. Jindal, W. Rhee, S. Vishwanath, S. A. Jafar, and A. Goldsmith, "Sum power iterative water-filling for multi-antenna gaussian broadcast channels," *IEEE Transactions on Information Theory*, vol. 51, no. 4, pp. 1570–1580, April 2005.
36 C. Oestges and B. Clerckx, *MIMO Wireless Communications: From Real-World Propagation to Space-Time Code Design*. Elsevier Science, 2010. [Online]. Available: https://books.google.fr/books?id=M3Yr9u3vrZ8C
37 E. Björnson and E. Jorswieck, "Optimal resource allocation in coordinated multi-cell systems," *Foundations and TrendsÂő in Communications and Information Theory*, vol. 9, no. 2âĂŞ3, pp. 113–381, 2013. [Online]. Available: http://dx.doi.org/10.1561/0100000069
38 A. O. Martìnez, E. D. Carvalho, and J. O. Nielsen, "Massive mimo properties based on measured channels: Channel hardening, user decorrelation and channel sparsity," in *2016 50th Asilomar Conference on Signals, Systems and Computers*, Nov 2016, pp. 1804–1808.
39 S. Cheng, D. P. Gaillot, E. Tanghe, P. Laly, T. Demol, W. Joseph, L. Martens, and M. Lienard, "Polarimetric distance-dependent models for large hall scenarios," *IEEE Transactions on Antennas and Propagation*, vol. 64, no. 5, pp. 1907–1917, May 2016.